Title

Reconciling early Deccan Traps CO2 outgassing and pre-KPB global climate

Journal

Proceedings of the National Academy of Sciences of the United States of America, 118(14)

ISSN

0027-8424

Authors

Nava, Andres Hernandez
Black, Benjamin A
Gibson, Sally A
et al.

Publication Date

2021-04-06

DOI

10.1073/pnas.2007797118

Peer reviewed

Reconciling early Deccan Traps CO_2 outgassing and pre-KPB global climate

Andres Hernandez Nava[a], Benjamin A. Black[a,b,1], Sally A. Gibson[c], Robert J. Bodnar[d], Paul R. Renne[e,f], and Loÿc Vanderkluysen[g]

[a]Department of Earth and Environmental Sciences, The Graduate Center of New York, City University of New York, New York, NY 10016; [b]Department of Earth and Atmospheric Sciences, The City College of New York, City University of New York, New York, NY 10031; [c]Department of Earth Sciences, University of Cambridge, CB2 3EQ Cambridge, United Kingdom; [d]Department of Geosciences, Virginia Tech, Blacksburg, VA 24060; [e]Department of Earth and Planetary Science, University of California, Berkeley, CA 94720-4767; [f]Berkeley Geochronology Center, Berkeley, CA 94709; and [g]Department of Biodiversity, Earth and Environmental Science, Drexel University, Philadelphia, PA 19104

Edited by Peter B. Kelemen, Lamont-Doherty Earth Observatory, Palisades, NY, and approved December 3, 2020 (received for review April 22, 2020)

A 2 to 4 °C warming episode, known as the Latest Maastrichtian warming event (LMWE), preceded the Cretaceous–Paleogene boundary (KPB) mass extinction at 66.05 ± 0.08 Ma and has been linked with the onset of voluminous Deccan Traps volcanism. Here, we use direct measurements of melt-inclusion CO_2 concentrations and trace-element proxies for CO_2 to test the hypothesis that early Deccan magmatism triggered this warming interval. We report CO_2 concentrations from NanoSIMS and Raman spectroscopic analyses of melt-inclusion glass and vapor bubbles hosted in magnesian olivines from pre-KPB Deccan primitive basalts. Reconstructed melt-inclusion CO_2 concentrations range up to 0.23 to 1.2 wt% CO_2 for lavas from the Saurashtra Peninsula and the Thakurvadi Formation in the Western Ghats region. Trace-element proxies for CO_2 concentration (Ba and Nb) yield estimates of initial melt concentrations of 0.4 to 1.3 wt% CO_2 prior to degassing. Our data imply carbon saturation and degassing of Deccan magmas initiated at high pressures near the Moho or in the lower crust. Furthermore, we find that the earliest Deccan magmas were more CO_2 rich, which we hypothesize facilitated more efficient flushing and outgassing from intrusive magmas. Based on carbon cycle modeling and estimates of preserved lava volumes for pre-KPB lavas, we find that volcanic CO_2 outgassing alone remains insufficient to account for the magnitude of the observed latest Maastrichtian warming. However, accounting for intrusive outgassing can reconcile early carbon-rich Deccan Traps outgassing with observed changes in climate and atmospheric pCO_2.

Deccan Traps | carbon release | magmatic outgassing | end-Cretaceous | paleoclimate

During emplacement of the voluminous intraplate magmatic systems known as Large Igneous Provinces (LIPs), dominantly basaltic magmas release volatiles at a scale that exceeds time-averaged outgassing from arc volcanoes by 1 to 2 orders of magnitude (e.g., ref. 1). Some LIPs coincide with major climate and carbon cycle disruptions, including the 252-Ma Siberian Traps (e.g., ref. 2) and the 201-Ma Central Atlantic Magmatic Province events (e.g., ref. 3). However, the existence and nature of a causal relationship between magmatic carbon release and carbon cycle perturbations remains controversial, in part because the CO_2 budget of LIP magmas and the contribution of metamorphic degassing are not well constrained (e.g., refs. 4–7). Estimating the timing and amount of CO_2 release from magmas is difficult because CO_2 saturation and degassing can initiate at near-Moho depths in basaltic magmatic systems (8). Consequently, inclusions trapped even in early-formed phenocrysts typically sample partially degassed melts with commensurately reduced CO_2 contents (9), and the timing of CO_2 release has the potential to decouple from rates of surface volcanism (10, 11). Moreover, for some LIPs, the amount of CO_2 released during magmatic degassing has been argued to be minor compared to that generated by metamorphic degassing from associated carbon-rich sedimentary wall rocks (e.g., refs. 5, 12). Early Deccan magmatism represents a strong test case for understanding the role of magmatic degassing because the crystalline Deccan country rocks are thought to be relatively volatile (carbon) poor (e.g., refs. 13–15). High-precision geochronology (16, 17) and paleoclimate records (18) track the timelines of both Deccan magmatism and Cretaceous–Paleogene environmental shifts.

The Deccan Traps LIP in India (Fig. 1) was emplaced in the late Cretaceous through early Paleogene, eventually erupting 0.6 to 1.3 × 10^6 km^3 of lava (19, 20). Previous studies have shown that the lava formations emplaced before the 66.05 ± 0.08 (1-σ) Ma Cretaceous Paleogene Boundary (KPB) correspond to ∼25% of the overall subaerial volume (16). In this paper, we refer to these pre-KPB lavas collectively as early Deccan volcanism. These lavas include the basalts and picrites in the Saurashtra region located in northwest India and the Kalsubai and Lonavala Subgroups in the Western Ghats region (Fig. 1). Available geochronology from the Saurashtra Peninsula carries large uncertainties (e.g., ref. 21), and the precise stratigraphic and temporal relationship between the Saurashtra lavas and Deccan volcanism in the Western Ghats is thus unclear. However, the overall Deccan age and geochemical progression from northwest to southeast (16, 17, 21, 22) have led previous workers (e.g., ref. 23) to interpret the lower lava units in Saurashtra region as among the earliest extrusive products of Deccan volcanism.

Significance

Carbon outgassing from Large Igneous Provinces has been invoked as a mechanism to drive major climate shifts throughout Earth's history. However, the lack of direct constraints on evolving carbon release from magmas in these provinces represents a major challenge for understanding the relationship between magmatism and environmental change. This paper presents constraints on CO_2 contents of early Deccan Traps lavas based on studies of olivine-hosted melt inclusions. We use these data to evaluate links between early Deccan carbon outgassing and an episode of pronounced warming just prior to the end-Cretaceous mass extinction. By accounting for evolving CO_2 budgets and degassing from intrusive magmas, this work quantitatively relates magma emplacement, outgassing, and observed changes in paleoclimate.

Author contributions: B.A.B. designed research; A.H.N. and B.A.B. performed research; S.A.G., R.J.B., P.R.R., and L.V. contributed new reagents/analytic tools; A.H.N., B.A.B., and R.J.B. analyzed data; and A.H.N., B.A.B., S.A.G., R.J.B., P.R.R., and L.V. wrote the paper.

The authors declare no competing interest.

This article is a PNAS Direct Submission.

[1]To whom correspondence may be addressed. Email: bblack@ccny.cuny.edu.

This article contains supporting information online at https://www.pnas.org/lookup/suppl/doi:10.1073/pnas.2007797118/-/DCSupplemental.

Published March 29, 2021.

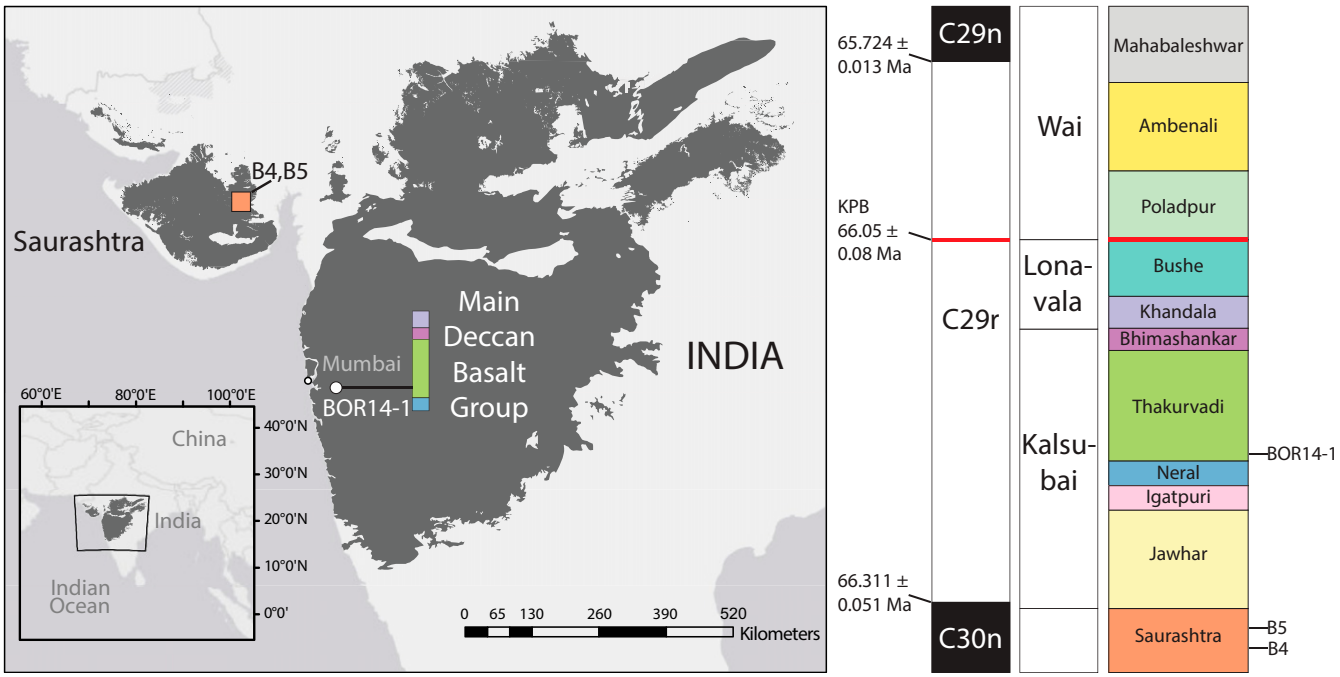

Fig. 1. Map showing the location and extent of Deccan Traps volcanism, including the Saurashtra region. The stratigraphic column shows Deccan formations and the position of melt inclusion samples in this study. The stratigraphic relationship between the Saurashtra region and the Main Deccan Traps section is uncertain, but the earliest Saurashtra lavas are thought to predate the main Deccan Basalt Group (21).

The warming episode that preceded the KPB, known as the Latest Maastrichtian warming event (LMWE), has been linked with the emplacement of the opening phases of Deccan volcanism (11, 16, 18, 24). This 2 to 4 °C warming event spanned ~300 ky just prior to the KPB (11, 18, 25). Latest Maastrichtian warming is reflected in multiple paleotemperature records in terrestrial and marine environments across both hemispheres (e.g., refs. 18, 25–27). High mercury concentrations just prior to the KPB have been interpreted as evidence for strong Deccan outgassing coinciding with the LMWE (28). However, the preserved subaerial volume of these early Deccan formations (~151 × 10^3 km^3) is much smaller than that of the subsequent Wai Subgroup (~461 × 10^3 km^3) (16, 20), challenging a straightforward link between volcanism and global warming. One possible explanation is that carbon release is not strictly proportional to lava volume owing to an evolving magmatic carbon budget and flushing of a CO_2-rich volatile phase, a process in which CO_2 exsolves at depth, decouples from the original magma, and rises through the magmatic system and country rocks, enriching shallower magma in exsolved CO_2 or degassing diffusely (e.g., refs. 6, 8, 10, 11, 16).

Despite evidence for a link between carbon release from the early Deccan volcanism and the LMWE, including a small (~0.5‰) negative shift in $\delta^{13}C$ (e.g., ref. 11), no direct constraints on the amount of CO_2 released during early Deccan volcanism exist. Existing petrologic data focus on magmatic sulfur and chlorine (29, 30). Choudhary et al. (31) measured CO_2 concentrations in post-KPB Wai Subgroup formations of 0.09 to 0.18 weight percent (wt%) CO_2. Prior estimates of ~0.5 wt% CO_2 in Deccan magmas (4, 32) are based on analogous modern eruptions of basalt, such as the Kilauea eruptions or the 1783 Laki fissure eruption in Iceland. Based on updated estimates of CO_2 contents of these basaltic eruptions (e.g., ref. 9), Black and Gibson (6) suggested the potential for some LIP magmas to carry 1 wt% CO_2 or more. Recently, evidence for 0.5 to 1 wt% CO_2 has also been reported for magmas from the Central Atlantic Magmatic Province (33).

In this study, we performed Raman (Fig. 2A) and NanoSIMS measurements of the CO_2 concentrations in glassy olivine-hosted melt inclusions (Fig. 2B) from primitive, MgO-rich lavas from the Saurashtra region (Fo_{84} to Fo_{88} olivines) and the Thakurvadi Formation in the Western Ghats (Fo_{73} to Fo_{80} olivines). We combined these data with trace element proxies for initial CO_2 contents of the melt prior to crystallization to quantify CO_2 release from early Deccan Traps magmas. We use our revised estimates to test the hypothesis that release of CO_2 from early Deccan volcanism was the primary driver of the LMWE. Our data also allow us to constrain minimum pressures of carbon saturation and to track initiation of degassing of Deccan Traps flood basalts.

Results

The total CO_2 concentration in the melt inclusions was reconstructed based on NanoSIMS data for the glass phase and Raman data for the vapor bubble, combined with an estimate of the volume percent vapor in the inclusion (Worksheet S1). We obtained CO_2 data from 43 bubble-bearing melt inclusions: 30 inclusions from two Saurashtra picrite lavas (B4 and B5, from the Botad drill core) and 13 inclusions from an olivine-bearing flow from the Thakurvadi Formation in the Western Ghats (BOR14-1). NanoSIMS analyses of 32 inclusions indicated CO_2 concentrations in glass ranging from 51 to 404 parts per million (ppm) ($n = 22$), with one outlier at 4,079 ppm, for Saurashtra inclusions and 18 to 239 ppm ($n = 10$) for the Thakurvadi inclusions (Worksheet S1).

Vapor bubbles analyzed by Raman indicate reconstructed CO_2 concentrations ranging from 195 to 11,740 ppm for the Saurashtra inclusions and from 60 to 9,880 ppm for the Thakurvadi inclusions (Worksheet S1), excluding one partially recrystallized inclusion as well as inclusions with vapor bubbles occupying >12 volume percent (implying they may represent inclusions that cotrapped melt and vapor; see *SI Appendix*, Figs. S1–S3). Each of these sample suites contained one inclusion with a vapor bubble occupying ~11 volume percent of the inclusion that significantly

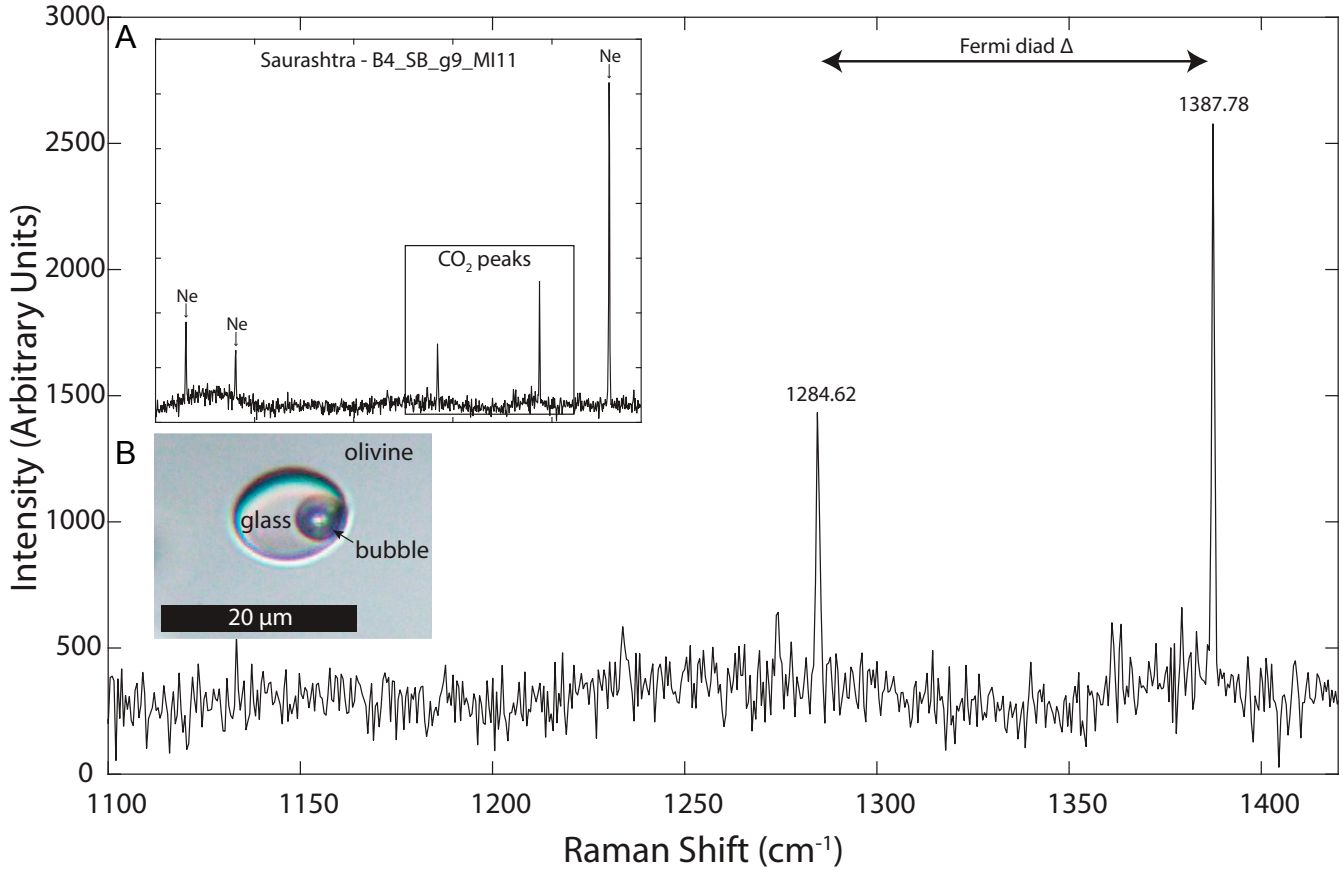

Fig. 2. Representative Raman spectrum for CO_2 showing the Fermi diad peaks that are located at 1,284.62 and 1,387.78 cm^{-1} in this example. The spacing between the two CO_2 peaks, Δ, is used to calculate the density of CO_2 in the bubble (68). The complete Raman spectrum of a melt inclusion (B4_SB_g9_MI11) along with the Ne lines that are used to calibrate the CO_2 peak positions (*A*), and the corresponding glassy, bubble-bearing melt inclusion is shown in inset (*B*).

increased the upper range of CO_2 concentrations. Given the uncertainties in bubble volume estimation and postentrapment cooling history (and thus expected shrinkage bubble size), the possibility that these bubbles were cotrapped with the melt cannot be excluded. Apart from these two inclusions, the maximum measured CO_2 in Saurashtra and Thakurvadi vapor bubbles was 7,770 and 2,300 ppm CO_2, respectively. Overall, vapor bubbles typically contained an order of magnitude more CO_2 than the glass, emphasizing the importance of quantifying CO_2 within bubbles as shown previously (9, 34).

It is well known that melt and fluid inclusions may reequilibrate following entrapment, resulting in changes in inclusion volume and/or composition. These processes include both plastic deformation of the host surrounding the melt inclusion via dislocation creep (35) as well as brittle deformation (decrepitation) of the host. While evidence of plastic deformation is difficult to recognize, we did not observe textural evidence for decrepitation of the melt inclusions. The lack of evidence for melt inclusion reequilibration could reflect a relatively slow ascent and cooling rate coupled with extensive postentrapment crystallization (36).

The trace elements Ba and Nb behave incompatibly during mantle melting, as does CO_2, but Ba and Nb do not degas from the melt as the pressure decreases during ascent and can therefore be used as proxies for the original CO_2 concentrations in the melt prior to degassing (6, 9, 37). In particular, Ba is commonly thought to be a robust proxy for CO_2 in primitive midocean ridge basalts (e.g., ref. 38). Because melt Ba concentrations are susceptible to crustal contamination (e.g., ref. 39), Nb serves as a useful check on Ba. We used mean Ba concentrations in melt inclusion glass from each sample to estimate the initial CO_2 concentration in the melt for Saurashtra and Thakurvadi magmas (Fig. 3). For other early Deccan formations, we used published whole-rock trace element data from lavas with >7 wt% MgO (40, 41) based on the assumption that more MgO-rich lavas likely experienced simpler, olivine-dominated fractionation histories (e.g., ref. 42). Published estimates of CO_2/Ba ratios span a large range, from 16 to 396 (43–45) (see *SI Appendix*, Fig. S5 and Table S2). We consider lower and higher CO_2/Ba ratios, performing example calculations using CO_2/Ba = 48.3 as reported in lavas from Borgarhraun, Iceland (38), as a lower estimate and a higher ratio of CO_2/Ba = 133 (37, 46) as an upper estimate for Deccan magmas.

Overall, CO_2 concentrations based on trace element proxies for CO_2 in conjunction with direct CO_2 measurements from melt inclusions from Saurashtra and Thakurvadi lavas support a general decline in initial CO_2 over the course of pre-KPB Deccan magmatism (Fig. 4*A*). Assuming conservative mantle CO_2/Ba ratios, mean Ba concentrations imply that Saurashtra magmas were initially CO_2 rich, with 0.5 to 1.3 wt% CO_2. Magmas from the Jawhar through Thakurvadi Formations initially contained ~0.4 wt% CO_2. Trace element ratios suggest Bushe Formation magmas that immediately predate the KPB [the Bushe–Poladpur transition has an interpolated age of ~66.03 ± 0.04 Ma (1-σ) (16)] carried only ~0.25 wt% CO_2. Published melt inclusion data from post-KPB formations indicate <0.2 wt% CO_2 (31).

We estimated melt inclusion minimum entrapment pressures using the VolatileCalc2.0 CO_2–H_2O solubility model (47). We combined measured CO_2 concentrations with measured H_2O where available (Worksheet S1). We assumed 0.5 wt% H_2O

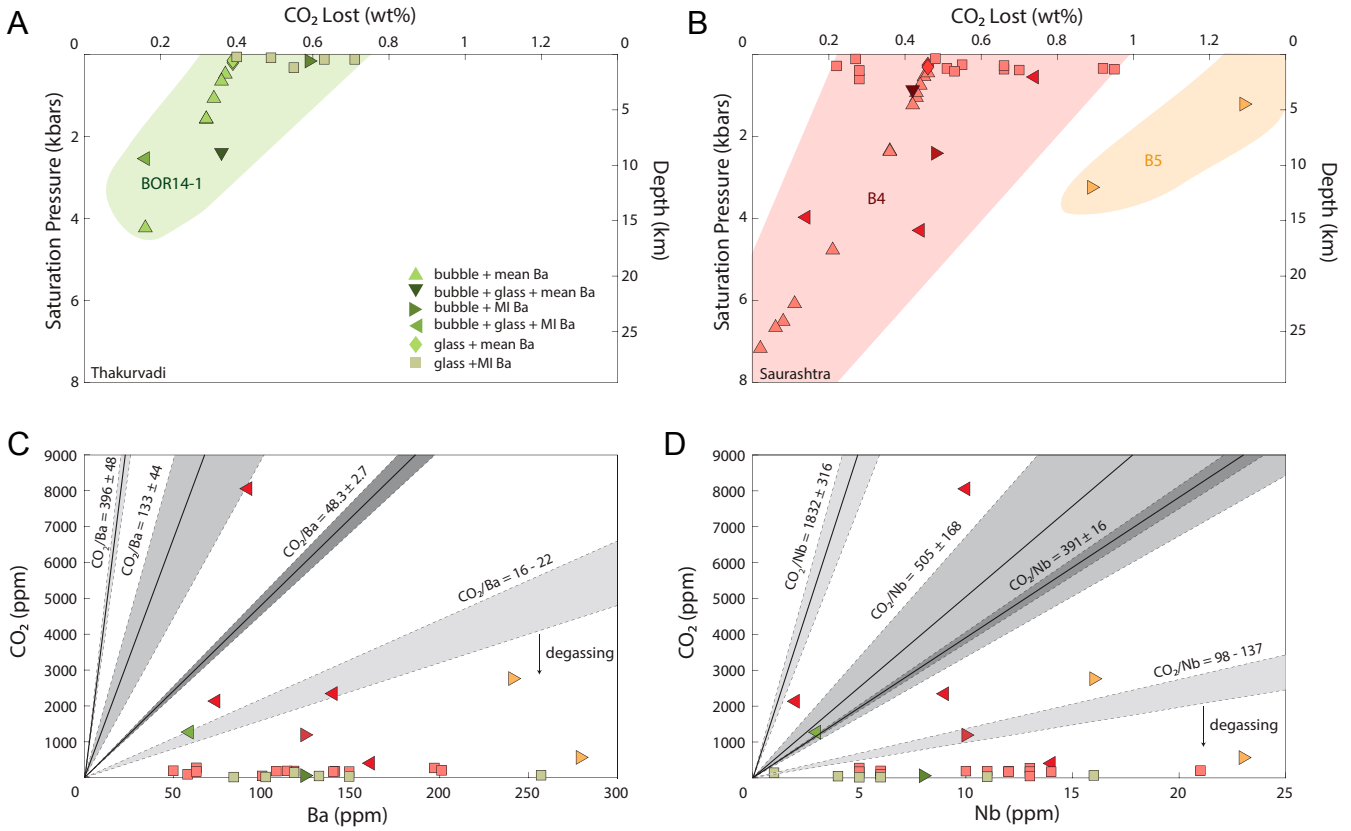

Fig. 3. CO_2 degassing trends for Deccan melt inclusions. The CO_2 lost to degassing at the time of melt inclusion entrapment is calculated as the difference between initial CO_2 based on Ba concentrations in each inclusion versus the reconstructed CO_2 concentration. Some melt inclusions lack trace-element data. For these inclusions, we used the mean Ba concentration in melt inclusions from that unit. We used VolatileCalc (47) to determine the saturation pressure of each melt inclusion (see text for details). (*A*) Melt inclusion data from the Thakurvadi Formation in the Western Ghats region. (*B*) Melt inclusion data from the Saurashtra region. (*C*) Saurashtra and Thakurvadi CO_2 versus Ba and (*D*) CO_2 versus Nb, compared with CO_2/Ba and CO_2/Nb ratios from refs. 37, 38, 43, 44.

(consistent with ref. 48) for melt inclusions without H_2O data. Melt inclusions from the Saurashtra lavas show minimum entrapment pressures of ~0.1 to 8 kbars, while the Thakurvadi melt inclusions show minimum entrapment pressures of ~0.1 to 4 kbars (with the exception of the two Saurashtra and Thakurvadi inclusions discussed above that contain ~1 wt% CO_2; estimated entrapment pressures for these inclusions are around 10 kbar). These pressures translate to minimum entrapment depths extending to ~30 and ~15 km, respectively (Fig. 3 *A* and *B*). Pressure estimates exceeding ~5 kbars incorporate additional uncertainty because VolatileCalc is not calibrated for pressures above 5 kbars. Estimates of initial melt CO_2 concentrations based on Ba and Nb abundances indicate that significant CO_2 degassing took place at depths greater than the estimated melt inclusion entrapment depths (Fig. 3 *A* and *B*), with the most CO_2-rich Deccan magmas likely reaching carbon saturation at the Moho or in the lower continental crust (Fig. 5). As they ascend into the crust, we expect stronger exsolution from more CO_2-rich magmas in response to pressure-dependent limitations on CO_2 solubility, facilitating more prevalent CO_2 flushing. Confirming this expectation, CO_2-rich Saurashtra magmas exsolved a higher proportion of their initial CO_2 than Thakurvadi magmas at an equivalent depth (Fig. 3 *A* and *B*).

Discussion

While melt inclusions provide valuable information concerning the preeruptive history of magmas, potential sources of uncertainty include determination of melt inclusion and vapor bubble dimensions (which are required to reconstruct the proportion of the total amount of CO_2 in the vapor bubble); mixed trapping of melt plus a volatile phase; uncertainty in assumed CO_2/Ba and CO_2/Nb ratios; and modification of these ratios due to crystallization, assimilation, and mixing processes (e.g., refs. 46, 49) in LIP magma reservoirs. Here, we discuss each of these factors in turn. As shown in *SI Appendix*, Fig. S1, slight differences in the measured volume proportion of vapor in the melt inclusions can affect the reconstructed CO_2 concentration by several hundred ppm, leading to uncertainties of ±5 to 10% (e.g., refs. 9, 50). We used the volume proportion of the melt inclusion occupied by the vapor bubble to distinguish between melt inclusions that trapped only melt and those that potentially trapped melt plus a volatile phase (*SI Appendix*, Figs. S2 and S3, see *Materials and Methods* and *SI Appendix*). In the absence of direct constraints on CO_2/Ba and CO_2/Nb in the Deccan mantle source (e.g., from undegassed melt inclusion suites), some uncertainty in CO_2/Ba and CO_2/Nb is unavoidable. Recent datasets from Iceland and popping rocks (43–45) provide evidence for mantle CO_2/Ba ratios extending up to CO_2/Ba = 396 and down to CO_2/Ba = 16, spanning a broader range than the values we use here to estimate initial CO_2 concentrations (*SI Appendix*, Fig. S5 and Table S2). For the Deccan, we disfavor lower CO_2/Ba = 16 to 22 as inferred from popping rocks (44) on the basis of our melt inclusion dataset. The Saurashtra inclusions with the highest CO_2/Ba (the maximum CO_2/Ba in our dataset was ~88; the mean of the three highest CO_2/Ba Saurashtra melt inclusions was 45 ± 38) yield a lower limit on CO_2/Ba in primitive Deccan magmas because degassing, crustal contamination, and crystallization prior to entrapment will decrease melt CO_2/Ba. This lower limit overlaps with the lower CO_2/Ba value we considered to estimate initial CO_2 (*SI Appendix*, Fig. S5),

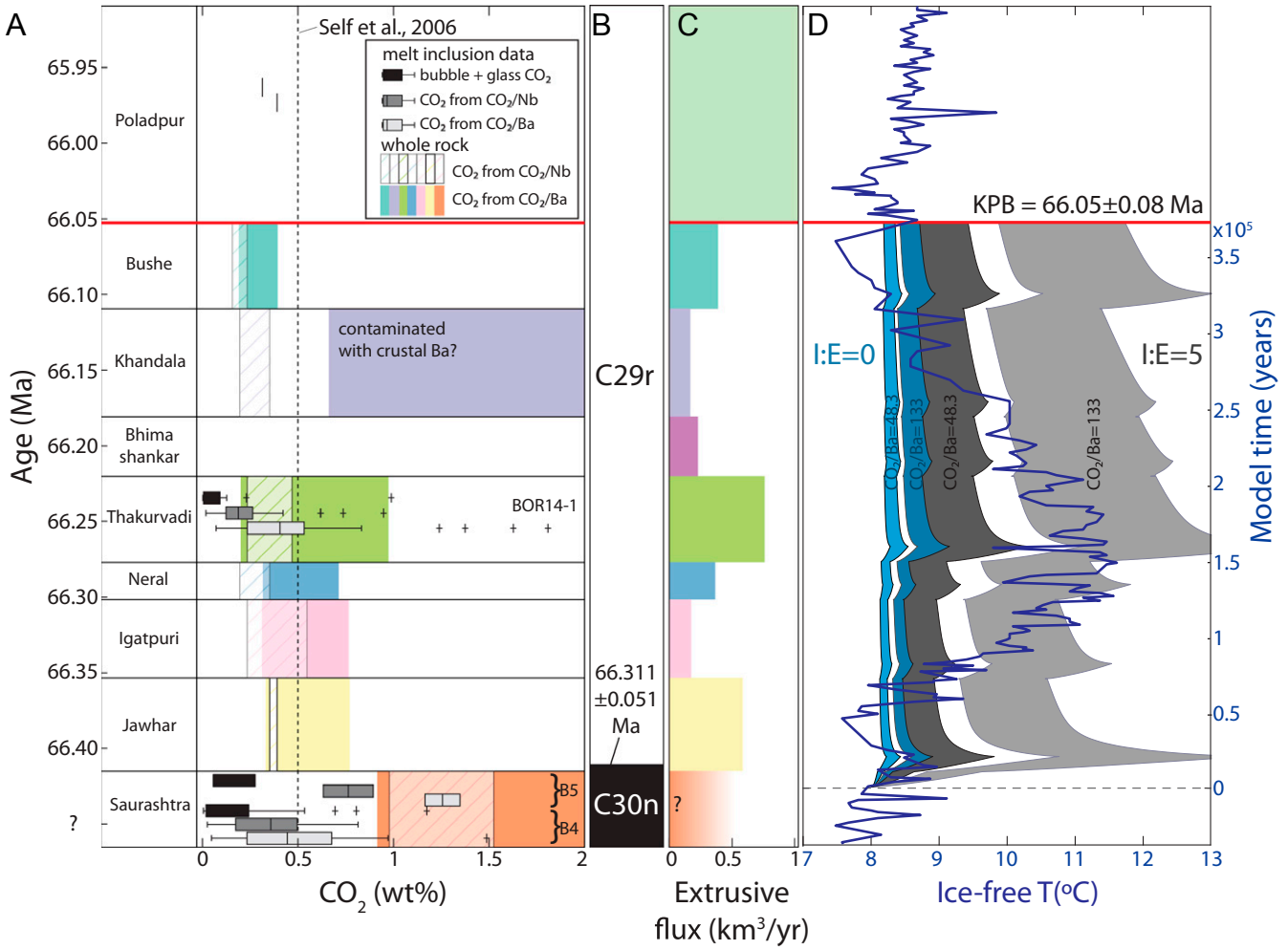

Fig. 4. Evolving CO_2 budgets for early Deccan Traps magmas and implications for latest Cretaceous climate. (*A*) CO_2 concentrations of Deccan melt inclusions and initial CO_2 concentrations based on trace element proxies from melt inclusion and whole-rock data, assuming $CO_2/Ba = 48.3$ and $CO_2/Nb = 391$ (38). Whole-rock trace element data from the Western Ghats region are from ref. 40. (*B*) Magnetostratigraphy from ref. 16. (*C*) The mean extrusive flux for each formation, calculated using the volumes estimated by ref. 20 and the age model of ref. 16. The duration of volcanism in the Saurashtra region is uncertain. (*D*) A comparison of observed changes in latest Maastrichtian climate with changes modeled with LOSCAR. Ocean temperatures are from a benthic $\delta^{18}O$ record from Integrated Ocean Drilling Program site 1262 on Walvis Ridge (18). LOSCAR results are shown for an I:E ratio of 0:1 (white) or 5:1 (blue shading), where the range reflects a climate sensitivity from 3 to 6 °C per doubling of CO_2 (75). Results are shown for lower and higher CO_2/Ba ratios (37, 38). See *Materials and Methods* and *SI Appendix* for details of LOSCAR modeling.

but we cannot rule out Deccan $CO_2/Ba > 133$ as measured in some Icelandic melt inclusion suites (43, 45).

As shown in Fig. 3, there is significant heterogeneity in Ba and Nb within melt inclusions from individual lavas. One possible explanation is that the relatively primitive magmas discussed here have not been strongly overprinted by cycles of recharge and mixing in deep LIP magma chambers, and trace element heterogeneity results from incomplete mixing of melts with different melting histories. If this interpretation is correct, the highest Ba concentrations from Saurashtra and Thakurvadi melt inclusions could reflect sampling of low degree melts with up to 2.2 wt% and 1.8 wt% CO_2, respectively. On the other hand, if fractionation or crustal contamination have also increased Ba concentrations in some inclusions, these inclusions could yield overestimates of CO_2. Because Saurashtra melt inclusions are hosted in very primitive olivines (up to Fo_{88}), significant fractionation appears unlikely, but fractionation prior to entrapment of Thakurvadi melt inclusions implies lower initial Ba concentrations than recorded in the melt inclusion population.

In addition to uncertainties in our estimates of magmatic CO_2 concentrations, the reconstruction of carbon outgassing fluxes introduces substantial uncertainties related to magma volume and degassing efficiency, particularly for intrusive magmas. Compared to the volumes of LIP magmas that erupt at the surface, a larger volume is probably emplaced and crystallized at depth (42). Concentrations of CO_2 and other volatiles in excess of the volatile solubility at these emplacement depths will be lost from the melt, forming a mobile exsolved phase that can contribute to the outgassing budget even if the melt in which these volatiles were originally dissolved does not erupt (e.g., refs. 9, 10). For example, Hartley et al. (9) estimated that intrusive magmas degassed around 60% of their initial CO_2 content during Iceland's Laki fissure eruption in 1783. The ratio of intrusive to extrusive magma volume, also known as the I:E ratio, is poorly constrained but may range from 1:1 to 10:1 for LIP magmas (e.g., ref. 51). Coffin and Eldholm (52) estimated an I:E ratio of 5:1 for the Deccan Traps based on seismic data.

In conjunction with our constraints on the evolving CO_2 budget of early Deccan magmas, we consider a range in the I:E to generate CO_2 fluxes to drive the Long-term Ocean Sediment CArbon Reservoir version 2.0.4 (LOSCAR) model. LOSCAR is a carbon cycle box model that tracks carbon exchange between the solid Earth,

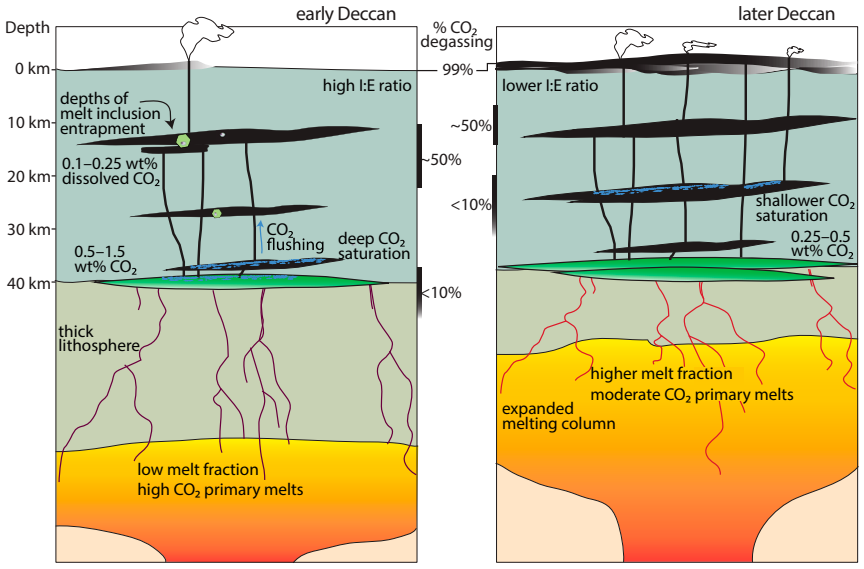

Fig. 5. A schematic showing CO_2 evolution from early (*Left*) to late (*Right*) Deccan based on initial CO_2 from trace elements and CO_2 saturation pressures. We hypothesize that declining initial CO_2 contents result from an expanding melting column and that higher initial CO_2 in the earliest Deccan magmas facilitated more efficient flushing and thus degassing of intrusive magmas. Adapted from ref. 8, with permission from Elsevier.

atmosphere, oceans, and sediments (53, 54). We use LOSCAR to compare the expected carbon cycle consequences of early Deccan carbon outgassing with records of sea surface temperature and pCO_2 (11, 18). We find that CO_2 outgassing from extrusive magmas alone is insufficient to explain the amplitude of the LMWE (Fig. 4*D*). Even with our revised CO_2 estimates, assumed CO_2/Ba = 133, and high assumed climate sensitivity of 6 °C per doubling of CO_2, the maximum warming from volcanic outgassing alone based on preserved subaerial volumes (19, 20) is ∼1 °C. Accounting for carbon release from intrusive magmas results in better agreement between predicted and observed climate shifts during the LMWE. We assume 60% degassing of intrusive magmas, conservative relative to the difference between initial and dissolved CO_2 in our most CO_2-rich inclusions and consistent with previous estimates for Laki (9). An I:E ratio of 5:1 drives maximum warming of 3 to 6 °C for a climate sensitivity of 3 to 6 °C per doubling of CO_2 (Fig. 4*D*), bookending the magnitude of warming during the LMWE.

The contribution from intrusive outgassing required to reproduce LMWE warming depends on the assumed undegassed CO_2/Ba ratio and the duration of early Deccan magmatism. With an I:E ratio of 5:1, carbon release calculated using conservative CO_2/Ba = 48.3 yields maximum warming that overlaps with only the low end of paleoclimate estimates, whereas CO_2/Ba = 133 yields maximum warming that overshoots paleoclimate estimates. If the actual Deccan CO_2/Ba ratio is close to the low end of this range, more intense intrusive outgassing (perhaps exceeding an I:E ratio of ∼5:1) may be required to align with the amplitude of LMWE warming. A smaller proportion of intrusive

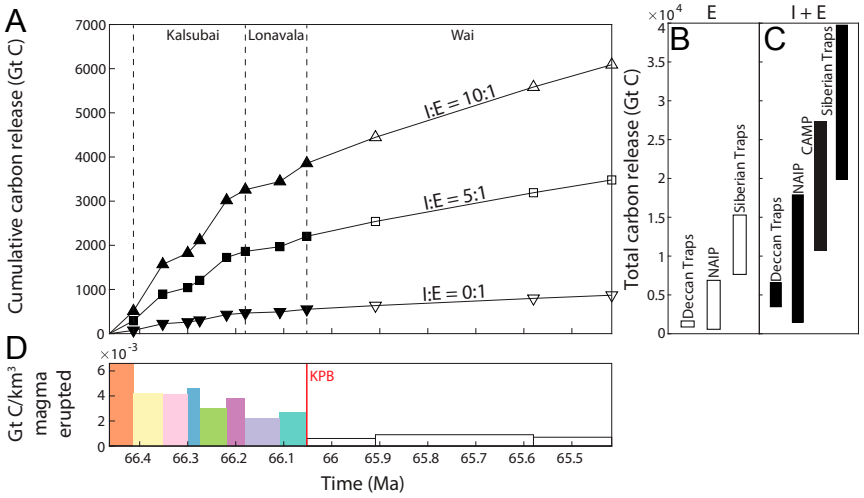

Fig. 6. Cumulative Deccan carbon release for a range of I:E magma-emplacement ratios. (*A*) Cumulative carbon contribution based on mean melt inclusion Ba concentrations from Saurashtra and Thakurvadi lavas, melt inclusions from the Wai subgroup from ref. 31, and whole-rock Ba data from the remaining formations from ref. 40. These calculations assume CO_2/Ba = 48.3 (38). Increasing the assumed CO_2/Ba ratio would increase carbon release estimates proportionally. See *SI Appendix*, Table S1 for details of calculations. Estimates of (*B*) extrusive carbon release and (*C*) intrusive plus extrusive carbon release from the Deccan Traps from this study compared with estimates from the Siberian Traps (55), the North Atlantic Igneous Province (55), and the Central Atlantic Magmatic Province (33). (*D*) The estimated carbon release per cubic kilometer of magma, assuming CO_2/Ba = 48.3 (38).

outgassing is implied if the actual CO_2/Ba ratio is closer to or exceeds the upper end of the range we considered, as may be the case during melting of plume-sourced material (43). For example, much higher Deccan CO_2/Ba = 396 (43) would reproduce the curve in Fig. 4 corresponding to CO_2/Ba = 133 and I:E = 5:1 with only a 1:2 I:E ratio. Consequently, if the early Deccan source mantle was very CO_2 rich, extrusive magmas could have played a more significant role in driving warming. The modeled carbon cycle response also depends on the tempo of magmatism. If the onset of early Deccan magmatism is taken to be ∼66.3 Ma based on the age of the Chron 30n-29r reversal and U-Pb ages for interbeds in the Jawhar Formation (17) rather than 66.41 Ma (16) as currently assumed (see *Materials and Methods*), the more compressed timeline for outgassing results in maximum atmospheric CO_2 levels that are ∼30% higher. Finally, although results from LOSCAR identify outgassing scenarios that yield broad agreement with paleoclimate records from the LMWE, significant differences remain between the structure of modeled and observed temperature evolution, particularly during the onset and waning of the LMWE. Our LOSCAR simulations assume a fixed I:E and uniform behavior of silicate weathering. In reality, these factors may vary through this interval, for example, due to a higher proportion of intrusive magmatism during the initial phases of Deccan emplacement (16) when the lithosphere was cold (Fig. 5), heterogeneous mantle CO_2/Ba as recently suggested for Iceland (45), and progressive exposure of easily weathered Deccan basalts (11). In addition to these factors, we suggest declining CO_2 budgets in the Khandala and Bushe Formations contributed to the waning of the LMWE coincident with eruption of these formations.

The degassing efficiency of intrusive magmas is as important as the I:E ratio for understanding potential climate consequences. Considering early intrusive magma suites as counterparts to the early Deccan volcanic formations studied here, our melt inclusion data imply that many early intrusive magmas could have been carbon rich, leading to carbon saturation and strong degassing, even for intrusions emplaced at lower-to-middle crustal depths. Consequently, we hypothesize that outgassing of deep intrusive magmas driven by CO_2 flushing was more prevalent during early Deccan magmatism (Fig. 5). Our work reinforces the view that considering only the volume or mass of extrusive rocks in determining the extent of LIP outgassing for volatiles such as carbon may significantly underestimate the total amount of outgassing.

Conclusions

We combined measurements of CO_2 concentrations in early Deccan Traps melt inclusions with trace element proxies for the abundance of magmatic CO_2 to quantify CO_2 release during early Deccan Traps magmatism. The concentration of CO_2 dissolved in Deccan melts at the time of melt inclusion entrapment reaches ∼1 wt% CO_2. Trace element proxies for initial melt concentrations imply that significant degassing occurred at depths greater than the middle to upper crust where melt inclusions were trapped.

Tracking the temporal variation in the amount of CO_2 released is critical to probing the relationship between LIP magmatism and global climate shifts. Melt inclusion and trace element data suggest that magmatic CO_2 budgets evolved through the course of Deccan magmatism, from initial concentrations of ∼1 wt% CO_2 in early Saurashtra melts to ∼0.4 wt% CO_2 in the Thakurvadi and ∼0.3 wt% CO_2 in the Bushe Formation, immediately prior to the KPB. This observation also supports the recent suggestion that LIP magmas may have highly variable CO_2 budgets and reach higher values than previous estimates of ∼0.5 wt% CO_2 (4, 6). Assuming a total Deccan extrusive volume of ∼600,000 km^3 (20), depending on the I:E ratio we estimate cumulative carbon release of 1,000 to 6,000 Gt C (Fig. 6*A*). This estimate is significantly lower than available estimates of carbon release from the Central Atlantic Magmatic Province and the Siberian Traps (33, 55) due both to the smaller cumulative volume of the Deccan Traps and our inference that voluminous Wai Subgroup formations carried less CO_2 than early Deccan magmas. Increasing the assumed CO_2/Ba ratio [calculations in Fig. 6 assume CO_2/Ba = 48.3 (38)] would increase carbon release estimates proportionally.

Based on our results, we infer that Deccan carbon outgassing is the most likely driver of climate shifts during the latest Maastrichtian. Similar changes in pCO_2 and sea surface temperatures are not clearly observed during the KPB extinction event (11, 27, 56), though some evidence for earliest Paleogene warming has been reported from fish debris from El Kef, Tunisia (56). Therefore, our results support the view that Deccan carbon outgassing did not play a major role in driving the KPB mass extinction itself (11, 16). In addition to carbon, Deccan sulfur release has also been considered as a driver for environmental stress (e.g., refs. 30, 57). Sulfur outgassing need not be proportional to carbon outgassing, in part because sulfur degassing is likely to take place much shallower in the magmatic system than carbon. Consequently, our results do not exclude the possibility that sulfur release from Wai Subgroup magmas contributed to climate disruption during the KPB mass extinction and its aftermath, including transient cooling on timescales not resolved in available paleoclimate records (20, 57–59).

Our revised CO_2 budget enables us to test the relationship between Deccan magmatism and a pronounced 2 to 4 °C warming interval in the Latest Maastrichtian commonly attributed to volcanism (e.g., refs. 11, 16, 18, 28). We use the LOSCAR carbon cycle model to investigate carbon release scenarios based on the preserved extrusive volumes of the opening phases of the Deccan Traps and a range of intrusive to extrusive ratios. Intrusive outgassing trades off with assumed mantle CO_2/Ba ratio and melt CO_2 prior to degassing. Higher CO_2/Ba implies less intrusive outgassing is required. Unless the Deccan source mantle was very CO_2 rich (43), we find that volcanic CO_2 outgassing alone remains insufficient to account for the magnitude of the observed latest Maastrichtian warming. Significant carbon release and flushing from magmas that did not erupt, possibly in combination with elevated latest Maastrichtian climate sensitivity, is required to relate early carbon-rich Deccan outgassing to the observed changes in climate and atmospheric pCO_2. Our findings underscore the importance of intrusive magmas for understanding the climate consequences of large igneous provinces.

Materials and Methods

Melt inclusions are small pockets of melt trapped during crystal growth that can record the magmatic conditions at the time of entrapment (60). They are one of the primary methods for CO_2 budget reconstruction in basaltic magmas (e.g., refs. 9, 61–63). Some melt inclusions contain vapor bubbles that form in response to the different thermal contraction behaviors of melt and host crystal following entrapment (60, 64). Further bubble growth can occur during postentrapment crystallization as silicate material is transferred from the melt phase to crystals, leading to volatile saturation and exsolution from the melt and into the vapor bubble (9, 34, 65). Measuring the amount of CO_2 sequestered by vapor bubbles is important for determining the preeruptive volatile content of the melt because bubbles can contain a large proportion (i.e., 40 to 90%) of the total CO_2 in the melt inclusion (9, 34, 66). Raman spectroscopy is commonly used to determine the CO_2 density in the bubble based on the distance between the CO_2 peaks nominally located at ∼1,285 cm^{-1} and ∼1,388 cm^{-1} (Fig. 2), jointly known as the Fermi diad (9, 34, 67, 68). The total CO_2 budget of the melt inclusion includes the CO_2 in vapor bubbles plus the CO_2 in the glass.

We identified glassy melt inclusions (glass phase and vapor bubble with no secondary crystal phases) hosted in highly forsteritic (Fo_{84} to Fo_{88}) olivine crystals from two lavas from the base of the Botad drill core in the Saurashtra Peninsula. The Botad, Wadhwan, and Dhandhuka cores in the Saurashtra Peninsula were drilled by the Geological Survey of India between 1924 and 1926, and the latter two cores reach the sedimentary rocks beneath the lava successions in this region (23, 41). These cores reveal a significant episode of picritic magmatism in the Saurashtra region, which is unusual for the Deccan province as a whole (23, 69). The petrography and

geochemistry of these cores were analyzed as described in refs. 23, 41, 69, and isotopic and additional trace element compositions were analyzed as described in ref. 70. These workers interpreted the lowest units on the Saurashtra Peninsula to be among the earliest products of Deccan volcanism. Available geochronology from the Saurashtra Peninsula carries large uncertainties, including an age of 66.0 ± 0.6 Ma (1-σ) for the base of the Botad core and 66.7 ± 0.5 Ma (1-σ) for the base of the Dhandhuka core (as recalculated in ref. 21), and further geochronologic data are needed to relate the timing of volcanism in the Saurashtra region to volcanism in the Western Ghats region. We also identified glassy melt inclusions (in Fo_{73} to Fo_{80} olivines) in a sample from the Thakurvadi Formation of the Kalsubai Subgroup that has been dated at 66.095 ± 0.047 (1-σ) Ma (16) (Fig. 1). We handpicked olivine grains hosting glassy melt inclusions using a petrographic microscope. Under reflected and transmitted light, the selected grains were polished until the inclusions were within 5 to 50 microns of the surface.

Raman spectroscopy was performed at Virginia Tech using a JY Horiba LabRam HR (800 mm) spectrometer equipped with a 100 mW 514 nm argon laser and 1,800 mm^{-1} grating while using a 100× microscope objective to focus on the vapor bubbles. A total of three 45 s scans were collected and then averaged for each vapor bubble. A Neon spectrum with known peak positions was collected simultaneously during each analysis and used for calibration (68). The density of the CO_2 in the vapor bubble was calculated using the procedure described by ref. 68. Building on work described by refs. 34 and 71, we used the bubble-to-melt volume fraction to distinguish between bubbles that formed after entrapment and those that represent trapping of a volatile phase and melt (known as "cotrapped" bubbles). We expect inclusions that consist only of trapped melt to show a relatively narrow range in the volume proportion of the melt inclusion occupied by the vapor bubble, with those that trapped melt plus vapor showing significant scatter to higher proportions of vapor. We test this prediction by calculating the vapor bubble volume fraction for a range of glass transition temperatures (34) and using a Deccan picrite composition from ref. 69. We also account for the effects of post entrapment crystallization (PEC) (*SI Appendix*, Fig. S3 and Worksheet S2). The calculated vapor bubble fractions agree with the measured vapor bubble fraction range for the majority of the melt inclusions studied here (*SI Appendix*, Figs. S2 and S3), except for five bubbles that are larger (12 to 30 volume percent). We therefore consider these five inclusions to contain cotrapped bubbles and exclude them from our CO_2 estimates. We also exclude one inclusion from sample B4 that is partially recrystallized.

Due to the size of the melt inclusions (in general less than 20 μm), volatile analysis of the glass was performed using the Cameca NanoSIMS 50L scanning ion microprobe at The Microanalysis Center for Geochemistry and Cosmochemistry at the California Institute of Technology. We measured major element glass compositions with the Cameca SX-100 5-spectrometer microprobe at the American Museum of Natural History. Postentrapment crystallization and Fe-loss correction was performed using the Petrolog-3 software (72). Initial FeO* for Saurashtra and Thakurvadi melt inclusions was estimated using the approach of ref. 73, which relies on empirical correlations between SiO_2 and FeO* for petrogenetically related magmas (*SI Appendix*, Fig. S4 and Appendix 1). Trace element compositions of the melt inclusions were determined by laser-ablation inductively coupled plasma mass spectroscopy at Virginia Tech using an Agilent 7500ce ICP-MS coupled with a Geolas 193 nm ArF laser ablation system. Both measured and postentrapment crystallization (PEC)-corrected trace element and volatile concentrations are given in Worksheet S1. PEC-corrected values were used in the text and to generate the figures and inputs to the LOSCAR carbon cycle model.

To calculate the original CO_2 concentrations of Deccan melts from Ba, we consider a lower ratio of CO_2/Ba = 48.3 ± 2.7 based on undegassed melt inclusions from Borgarhraun, Iceland (38), as well as a higher ratio of CO_2/Ba = 133 ± 44 from ref. 37. The latter value is also motivated by the possibility that values from Borgarhraun underestimate mantle CO_2/Ba ratios due to mixing of primary and undegassed melts (46). Heterogeneous mantle CO_2/Ba is possible; values substantially higher than CO_2/Ba = 133 have been inferred for some regions of the mantle beneath Iceland (45). In Fig. 3 *C* and *D* we compare these CO_2/Ba ratios (as well as CO_2/Nb) with data from our melt inclusions. Almost all melt inclusions show maximum CO_2/Ba and CO_2/Nb values that are degassed to varying extents relative to primitive mantle-derived ratios. The Saurashtra melt inclusions with the highest CO_2/Ba and CO_2/Nb ratios extend to higher values than ratios from Borgarhraun (Fig. 3 *C* and *D*). Because degassing lowers melt CO_2 and crystallization increases melt concentrations of incompatible elements such as Ba and Nb, these values represent potential lower limits on primitive Deccan CO_2/Ba and CO_2/Nb. Fo_{73} to Fo_{80} Thakurvadi olivines reflect melts that have likely undergone more fractionation than Saurashtra melts prior to melt inclusion entrapment, implying the Saurashtra samples provide a more meaningful lower limit on Deccan CO_2/Ba and CO_2/Nb.

LOSCAR was configured for Paleogene geography, including a Tethys basin (53, 54). Outgassing was specified based on published eruptive volume estimates and geochronology (16, 17, 20, 74) and estimates of the CO_2 budget for each formation from this work. We consider a range in CO_2/Ba ratios based on the range in published values to estimate CO_2 release. For the Bhimashankar Formation, in the absence of trace element data from MgO-rich lavas, we assume 0.5 wt% CO_2 (4). For the Khandala Formation, which displays high Ba/Nb ratios, we use Nb as a proxy for CO_2 rather than Ba. The relationship between changes in radiative forcing due to variations in the CO_2 concentration in the atmosphere and changes in surface temperature, known as the climate sensitivity, varies through time. Farnsworth et al. (75) suggested that climate sensitivity in the latest Cretaceous was high, with average global temperature increasing by 5.5 °C for every two-fold increase in CO_2 concentration. We consider a range of climate sensitivity from 3 to 6 °C per doubling of CO_2. Finally, we also examine a range of I:E ratios from 0 to 10:1 to investigate the potential impact of carbon release from intrusive magmas.

Data Availability. All study data are included in the article and/or supporting information.

ACKNOWLEDGMENTS. We acknowledge funding from NSF Grants IES-1615147, 1615003, and 1615021 and the Chleck Family Foundation. We thank the editor and two anonymous reviewers for insightful feedback that improved this manuscript. We thank Lowell Moore, Charles Farley, Luca Fedele, Brian Monteleone, Yunbin Guan, Adrian Fiege, Jim Webster, Celine Martin, and Keiji Hammond for discussions and assistance with sample analysis. We thank Tushar Mittal, Courtney Sprain, Anja Schmidt, Michael Manga, Mark Richards, Steve Self, and the members of the City Volcano Lab at City University of New York for insightful discussions that influenced this work.

1. C. A. Suarez, M. Edmonds, A. P. Jones, Earth catastrophes and their impact on the carbon cycle. *Elements* **15**, 301–306 (2019).
2. S. D. Burgess, J. D. Muirhead, S. A. Bowring, Initial pulse of Siberian Traps sills as the trigger of the end-Permian mass extinction. *Nat. Commun.* **8**, 164 (2017).
3. A. Bachan, J. L. Payne, Modelling the impact of pulsed CAMP volcanism on pCO_2 and $\delta^{13}C$ across the Triassic-Jurassic transition. *Geol. Mag.* **153**, 252–270 (2016).
4. S. Self, M. Widdowson, T. Thordarson, A. E. Jay, Volatile fluxes during flood basalt eruptions and potential effects on the global environment: A Deccan perspective. *Earth Planet. Sci. Lett.* **248**, 518–532 (2006).
5. H. Svensen *et al.*, Siberian gas venting and the end-Permian environmental crisis. *Earth Planet. Sci. Lett.* **277**, 490–500 (2009).
6. B. A. Black, S. A. Gibson, Deep carbon and the life cycle of large igneous provinces. *Elements* **15**, 319–324 (2019).
7. T. S. Tobin, C. M. Bitz, D. Archer, Modeling climatic effects of carbon dioxide emissions from Deccan Traps volcanic eruptions around the Cretaceous–Paleogene boundary. *Palaeogeogr. Palaeoclimatol. Palaeoecol.* **478**, 139–148 (2017).
8. B. A. Black, M. Manga, Volatiles and the tempo of flood basalt magmatism. *Earth Planet. Sci. Lett.* **458**, 130–140 (2017).
9. M. E. Hartley, J. Maclennan, M. Edmonds, T. Thordarson, Reconstructing the deep CO_2 degassing behaviour of large basaltic fissure eruptions. *Earth Planet. Sci. Lett.* **393**, 120–131 (2014).
10. D. I. Armstrong McKay, T. Tyrrell, P. A. Wilson, G. L. Foster, Estimating the impact of the cryptic degassing of large igneous provinces: A mid-Miocene case-study. *Earth Planet. Sci. Lett.* **403**, 254–262 (2014).
11. P. M. Hull *et al.*, On impact and volcanism across the Cretaceous-Paleogene boundary. *Science* **367**, 266–272 (2020).
12. C. Ganino, N. T. Arndt, Climate changes caused by degassing of sediments during the emplacement of large igneous provinces. *Geology* **37**, 323–326 (2009).
13. K. L. Kaila, P. R. K. Murty, V. K. Rao, G. E. Kharetchko, Crustal structure from deep seismic soundings along the Koyna II (Kelsi-Loni) profile in the Deccan Trap area, India. *Tectonophysics* **73**, 365–384 (1981).
14. S. K. Biswas, Regional tectonic framework, structure and evolution of the western marginal basins of India. *Tectonophysics* **135**, 307–327 (1987).
15. H. C. Sheth, "From Deccan to Réunion: No trace of a mantle plume" in *Plates, Plumes, and Paradigms*, G. R. Foulger, J. H. Natland, D. C. Presnall, D. L. Anderson, Eds. (Special Papers - Geological Society of America, 2005), vol. 388, pp. 477–501.
16. C. J. Sprain *et al.*, The eruptive tempo of Deccan volcanism in relation to the Cretaceous-Paleogene boundary. *Science* **363**, 866–870 (2019).
17. B. Schoene *et al.*, U-Pb constraints on pulsed eruption of the Deccan Traps across the end-Cretaceous mass extinction. *Science* **363**, 862–866 (2019).
18. J. S. K. Barnet *et al.*, A new high-resolution chronology for the late Maastrichtian warming event: Establishing robust temporal links with the onset of Deccan volcanism. *Geology* **46**, 147–150 (2018).

19. A. Jay, M. Widdowson, Stratigraphy, structure and volcanology of the SE deccan continental flood basalt province: Implications for eruptive extent and volumes. *J. Geol. Soc. London* **165**, 177–188 (2008).
20. M. A. Richards *et al*., Triggering of the largest Deccan eruptions by the Chicxulub impact. *Geol. Soc. Am. Bull.* **127**, 1507–1520 (2015).
21. L. Parisio *et al*., ^{40} Ar/^{39} Ar ages of alkaline and tholeiitic rocks from the northern Deccan Traps: Implications for magmatic processes and the K–Pg boundary. *J. Geol. Soc. London* **173**, 679–688 (2016).
22. R. K. Srivastava, F. Wang, S. Wenbei, Substantiation of reunion plume induced prolonged magmatic pulses (ca. 70.5–65.5 Ma) of the Deccan LIP in the Chhotanagpur gneissic complex, eastern India: Constraints from 40Ar/39Ar geochronology. *J. Earth Syst. Sci.* **129**, 95–104 (2020).
23. P. Krishnamurthy, K. G. Cox, Picrite basalts and related lavas from the Deccan Traps of Western India. *Contrib. Mineral. Petrol.* **62**, 53–75 (1977).
24. R. K. Olsson, J. D. Wright, K. G. Miller, Paleobiogeography of Pseudotextularia elegans during the latest Maastrichtian global warming event. *J. Foraminiferal Res.* **31**, 275–282 (2001).
25. L. Woelders *et al*., Robust multi-proxy data integration, using late Cretaceous paleotemperature records as a case study. *Earth Planet. Sci. Lett.* **500**, 215–224 (2018).
26. S. V. Petersen, A. Dutton, K. C. Lohmann, End-Cretaceous extinction in Antarctica linked to both Deccan volcanism and meteorite impact via climate change. *Nat. Commun.* **7**, 12079 (2016).
27. M. J. Henehan, P. M. Hull, D. E. Penman, J. W. B. Rae, D. N. Schmidt, Biogeochemical significance of pelagic ecosystem function: An end-Cretaceous case study. *Philos. Trans. R. Soc. Lond. B Biol. Sci.* **371**, 20150510 (2016).
28. K. W. Meyer *et al*., Biogenic carbonate mercury and marine temperature records reveal global influence of Late Cretaceous Deccan Traps. *Nat. Commun.* **10**, 5356 (2019).
29. S. Callegaro *et al*., Microanalyses link sulfur from large igneous provinces and Mesozoic mass extinctions. *Geology* **42**, 895–898 (2014).
30. S. Self, S. Blake, K. Sharma, M. Widdowson, S. Sephton, Sulfur and chlorine in late Cretaceous Deccan magmas and eruptive gas release. *Science* **319**, 1654–1657 (2008).
31. B. R. Choudhary, M. Santosh, B. De Vivo, G. Jadhav, E. V. S. S. K. Babu, Melt inclusion evidence for mantle heterogeneity and magma degassing in the Deccan large Igneous Province, India. *Lithos* **346–347**, 105135 (2019).
32. A. L. Chenet *et al*., Determination of rapid Deccan eruptions across the Cretaceous-Tertiary boundary using paleomagnetic secular variation: 2. Constraints from analysis of eight new sections and synthesis for a 3500-m-thick composite section. *J. Geophys. Res.* **114**, B06103 (2009).
33. M. Capriolo *et al*., Deep CO_2 in the end-Triassic Central Atlantic Magmatic province. *Nat. Commun.* **11**, 1670 (2020).
34. L. R. Moore *et al*., Bubbles matter: An assessment of the contribution of vapor bubbles to melt inclusion volatile budgets. *Am. Mineral.* **100**, 806–823 (2015).
35. F. Schiavi, A. Provost, P. Schiano, N. Cluzel, P-V-T-X evolution of olivine-hosted melt inclusions during high-temperature homogenization treatment. *Geochim. Cosmochim. Acta* **172**, 1–21 (2016).
36. J. Maclennan, Bubble formation and decrepitation control the CO_2 content of olivine-hosted melt inclusions. *Geochem. Geophys. Geosyst.* **18**, 597–616 (2017).
37. A. Rosenthal, E. H. Hauri, M. M. Hirschmann, Experimental determination of C, F, and H partitioning between mantle minerals and carbonated basalt, CO_2/Ba and CO_2/Nb systematics of partial melting, and the CO_2 contents of basaltic source regions. *Earth Planet. Sci. Lett.* **412**, 77–87 (2015).
38. E. H. Hauri *et al*., CO_2 content beneath northern Iceland and the variability of mantle carbon. *Geology* **46**, 55–58 (2018).
39. A. Kent, J. Baker, M. Wiedenbeck, Contamination and melt aggregation processes in continental flood basalts: Constraints from melt inclusions in oligocene basalts from Yemen. *Earth Planet. Sci. Lett.* **202**, 577–594 (2002).
40. J. E. Beane, "Flow stratigraphy, chemical variation and petrogenesis of Deccan flood basalts from the Western Ghats, India," PhD dissertation, Washington State Univ., Pullman, WA (1988).
41. P. Krishnamurthy, "Petrological and chemical studies of Deccan Trap lavas from western India," PhD dissertation, Univ. Edinburgh., Edinburgh, UK (1974).
42. K. G. Cox, A model for flood basalt vulcanism. *J. Petrol.* **21**, 629–650 (1980).
43. W. G. R. Miller *et al*., Estimating the carbon content of the deep mantle with Icelandic melt inclusions. *Earth Planet. Sci. Lett.* **523**, 115699 (2019).
44. M. R. Jones *et al*., New constraints on mantle carbon from Mid-Atlantic Ridge popping rocks. *Earth Planet. Sci. Lett.* **511**, 67–75 (2019).
45. S. Matthews, O. Shorttle, J. Maclennan, J. F. Rudge, The global melt inclusion C/Ba array: Mantle variability, melting process, or degassing? *Geochim. Cosmochim. Acta* **293**, 525–543 (2020).
46. S. Matthews, O. Shorttle, J. F. Rudge, J. Maclennan, Constraining mantle carbon: CO_2-trace element systematics in basalts and the roles of magma mixing and degassing. *Earth Planet. Sci. Lett.* **480**, 1–14 (2017).
47. S. Newman, J. B. Lowenstern, VolatileCalc: A silicate melt–H_2O–CO_2 solution model written in visual basic for excel. *Comput. Geosci.* **28**, 597–604 (2002).
48. J. A. Cabato, C. J. Stefano, S. B. Mukasa, Volatile concentrations in olivine-hosted melt inclusions from the Columbia River flood basalts and associated lavas of the Oregon Plateau: Implications for magma genesis. *Chem. Geol.* **392**, 59–73 (2015).
49. K. Shimizu, A. E. Saal, E. H. Hauri, M. R. Perfit, R. Hékinian, Evaluating the roles of melt-rock interaction and partial degassing on the CO_2/Ba ratios of MORB: Implications for the CO_2 budget in the Earth's depleted upper mantle. *Geochim. Cosmochim. Acta* **260**, 29–48 (2019).
50. L. R. Moore, N. Mironov, M. Portnyagin, E. Gazel, R. J. Bodnar, Volatile contents of primitive bubble-bearing melt inclusions from Klyuchevskoy volcano, Kamchatka: Comparison of volatile contents determined by mass-balance versus experimental homogenization. *J. Volcanol. Geotherm. Res.* **358**, 124–131 (2018).
51. V. A. Ridley, M. A. Richards, Deep crustal structure beneath large igneous provinces and the petrologic evolution of flood basalts. *Geochem. Geophys. Geosyst.* **11**, Q09006 (2010).
52. M. F. Coffin, O. Eldholm, Large igneous provinces: Crustal structure, dimensions, and external consequences. *Rev. Geophys.* **32**, 1–36 (1994).
53. R. E. Zeebe, LOSCAR: Long-term Ocean-atmosphere-Sediment CArbon cycle reservoir model v2.0.4. *Geosci. Model Dev.* **5**, 149–166 (2012).
54. R. E. Zeebe, A. Ridgwell, J. C. Zachos, Anthropogenic carbon release rate unprecedented during the past 66 million years. *Nat. Geosci.* **9**, 325–329 (2016).
55. A. D. Saunders, Two LIPs and two Earth-system crises: The impact of the North Atlantic igneous province and the Siberian Traps on the Earth-surface carbon cycle. *Geol. Mag.* **153**, 201–222 (2016).
56. K. G. MacLeod, P. C. Quinton, J. Sepúlveda, M. H. Negra, Postimpact earliest Paleogene warming shown by fish debris oxygen isotopes (El Kef, Tunisia). *Science* **360**, 1467–1469 (2018).
57. A. Schmidt *et al*., Selective environmental stress from sulphur emitted by continental flood basalt eruptions. *Nat. Geosci.* **9**, 77–82 (2016).
58. E. Font *et al*., Atmospheric halogen and acid rains during the main phase of Deccan eruptions: Magnetic and mineral evidence. Volcanism, impacts, and mass extinctions: Causes and effects. *Spec. Pap. Geol. Soc. Am.* **505**, 353–368 (2014).
59. B. A. Black *et al*., Systemic swings in end-Permian climate from Siberian Traps carbon and sulfur outgassing. *Nat. Geosci.* **11**, 949–954 (2018).
60. N. Métrich, P. J. Wallace, Volatile abundances in basaltic magmas and their degassing paths tracked by melt inclusions. *Rev. Mineral. Geochem.* **69**, 363–402 (2008).
61. P. Wallace, V. Kamenetsky, P. Cervantes, Melt inclusion CO_2 contents, pressures of olivine crystallization, and the problem of shrinkage bubbles. *Am. Mineral.* **100**, 787–794 (2015).
62. E. Bali, M. E. Hartley, S. A. Halldórsson, G. H. Gudfinnsson, S. Jakobsson, Melt inclusion constraints on volatile systematics and degassing history of the 2014–2015 Holuhraun eruption, Iceland. *Contrib. Mineral. Petrol.* **173**, 9 (2018).
63. L. R. Moore, R. J. Bodnar, A pedagogical approach to estimating the CO_2 budget of magmas. *J. Geol. Soc. London* **176**, 398–407 (2019).
64. J. B. Lowenstern, "Applications of silicate-melt inclusions to the study of magmatic volatiles" in *Magmas, Fluids and Ore Deposition*, J. F. H. Thompson, Ed. (Mineral. Assoc. Canada, Quebec, 1995), pp. 71–99.
65. M. Steele-MacInnis, R. Esposito, L. R. Moore, M. E. Hartley, Heterogeneously entrapped, vapor-rich melt inclusions record pre-eruptive magmatic volatile contents. *Contrib. Mineral. Petrol.* **172**, 18 (2017).
66. M. Steele-Macinnis, R. Esposito, R. J. Bodnar, Thermodynamic model for the effect of post-entrapment crystallization on the H_2O-CO_2 systematics of vapor-saturated, silicate melt inclusions. *J. Petrol.* **52**, 2461–2482 (2011).
67. K. M. Rosso, R. J. Bodnar, Microthermometric and Raman spectroscopic detection limits of CO_2 in fluid inclusions and the Raman spectroscopic characterization of CO_2. *Geochim. Cosmochim. Acta* **59**, 3961–3975 (1995).
68. H. M. Lamadrid *et al*., Reassessment of the Raman CO_2 densimeter. *Chem. Geol.* **450**, 210–222 (2017).
69. P. Krishnamurthy, K. Gopalan, J. D. Macdougall, Olivine compositions in picrite basalts and the deccan volcanic cycle. *J. Petrol.* **41**, 1057–1069 (2000).
70. Z. X. Peng, J. J. Mahoney, Drillhole lavas from the northwestern Deccan Traps, and the evolution of Réunion hotspot mantle. *Earth Planet. Sci. Lett.* **134**, 169–185 (1995).
71. J. M. Riker, "The 1859 eruption of Mauna Loa volcano, Hawai'i: Controls on the development of long lava channels," MS thesis, University of Oregon, Eugene, OR (2005).
72. L. V. Danyushevsky, P. Plechov, Petrolog3: Integrated software for modeling crystallization processes. *Geochem. Geophys. Geosyst.* **12**, 1–32 (2011).
73. M. A. Longpré, A. Klügel, A. Diehl, J. Stix, Mixing in mantle magma reservoirs prior to and during the 2011-2012 eruption at El Hierro, Canary Islands. *Geology* **42**, 315–318 (2014).
74. P. R. Renne *et al*., State shift in Deccan volcanism at the Cretaceous-Paleogene boundary, possibly induced by impact. *Science* **350**, 76–78 (2015).
75. A. Farnsworth *et al*., Climate sensitivity on geological timescales controlled by nonlinear feedbacks and Ocean circulation. *Geophys. Res. Lett.* **46**, 9880–9889 (2019).